# The Characterization of Photoinduced Chirality in a Liquid-Crystalline Azo Polymer on Irradiation with Circularly Polarized Light

**Dennis K. Hore[†] and Almeria L. Natansohn**

*Department of Chemistry, Queen's University, Kingston ON, K7L 3N6, Canada*

**Paul L. Rochon***

*Department of Physics, Royal Military College, P.O. Box 17000, Station Forces, Kingston ON, K7L 7B4, Canada*

*Received: October 2, 2002; In Final Form: December 6, 2002*

In this study, an achiral liquid-crystalline azo polymer is irradiated with circularly polarized light, and the transmitted polarization data show evidence of photoinduced chirality. When the polarization of the laser is switched from left- to right-handed, the chirality of the polymer film is switched as well. In a more revealing experiment, the handedness of the laser is fixed and the evolution of the ordering is monitored. Two models are described to interpret this result, one based on a uniaxial arrangement with the observed circular anisotropy included on a phenomenological level; the other based on a helical arrangement of chromophores. These models were used to fit the polarization data in order to determine the anisotropic optical constants that characterize the structural arrangement. It was noticed that during the irradiation, the sense of the circular anisotropy switches. This is also discussed in relation to both models presented.

## 1. Introduction

When polymers containing photochromic azobenzene moieties in their side chains are irradiated with linearly-polarized light, in-plane uniaxial ordering results from the motion induced by multiple trans−cis−trans isomerization cycles and the subsequent angular trapping that occurs when the transition dipole moments fall perpendicular to the polarization axis of the laser.[1−5] The resulting linear arrangement of chromophores has potential for use in optical switching[6−9] and storage applications.[10−13] Over the past two decades, there has been much interest in using light to trigger changes in chiral systems[14] and, in particular, using azo dyes to modulate an existing chirality.[15−25] Now, interest has developed in generating chiral structures by means of photoalignment through isomerization of azo groups.

The phenomenon of photoinduced chirality in an achiral azo polymer was first demonstrated by Nikolova et al. in 1997[26] when they exposed a liquid-crystalline azo polymer to circularly polarized light. At that time, before any mechanism was proposed, it was believed that liquid-crystallinity was an essential factor for the material to exhibit such behavior. At the same time, they noticed that holographic gratings prepared with a similar material displayed unusual properties, attributed to the presence of the circular anisotropy.[27] Shortly afterward, they published a more detailed study where a similar polymer was exposed to circularly polarized light.[28] At this point, Nikolova et al. proposed that the chromophore-bearing side chains have a tendency to orient themselves normal to the film surface during long exposures. Since they are tethered to the polymer backbone, however, they cannot accomplish free rotation but instead precess around the film normal, thereby creating a helix. At this point the authors also suggested that the relation $nP\Delta n_{\mathrm{lin}} < \lambda$ was true for the induced structures, and so used the de Vries relation[15] to discuss the rotatary power.

In 2000, Iftime et al. have studied a liquid-crystalline azo polymer that was annealed to trap its smectic A phase at room temperature, where it was irradiated with right- and then left-circularly polarized light.[29] CD spectra were obtained using a commercial CD spectrophotometer and band assignments were made based on CD studies of similar materials[30] in accordance with the chiral exciton coupling rules.[31] After observing a change in the sign of the bands when the handedness of the pump beam was switched from left to right, the authors concluded that the resulting helix was correspondingly erased and then reinscribed with opposite handedness. This provided the first account of photoswitching optically induced chirality.

In the same year, Ivanov et al. have demonstrated that liquid crystallinity is not a requirement and that chirality can also be induced in amorphous azo polymers if they are prealigned with linearly polarized light.[32] Irradiating with vertical or horizontal light before the circularly polarized light has proven that the sign and value of the optical rotation does not depend on the direction of the previously induced optical axis. The next publication from Nikolova's group quantitatively showed that the induced rotation depends on the ellipticity of the pump.[33] Here they have used Azzam and Bashara's formalism[34] to describe the propagation of polarized light through a helix. The amorphous polymers in this study behaved exactly in accordance with the predictions of this theory, further lending evidence to the idea that a macroscopic helix is being inscribed. The authors have extended their investigation using this model to describe the general case of inducing circular anisotropy with one wavelength and measuring with another.[35] The culmination of all these results now provided much evidence for a more

* Corresponding author. E-mail: rochon-p@rmc.ca. Phone: 613-541-6000 ext 6451. Fax: 613-541-6040.

[†] Present address: Department of Chemistry, University of Oregon, Eugene OR, 97403.

10.1021/jp0271209 CCC: $25.00 
Published on Web 02/22/2003

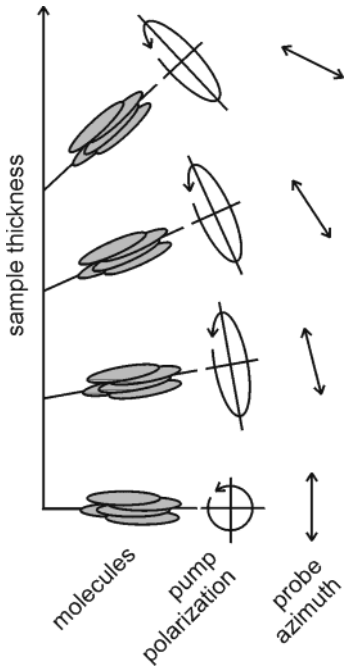


**Figure 1.** Self-rotation of the polarization ellipse as a result of interaction with an anisotropic distribution of chromophores. The chromophores respond to the light polarization and the light polarization responds to the chromophores.

descriptive model, first proposed by Nikolova et al.[33] It is imagined that the sample consists of many layers, with linear anisotropy present in each layer. When circularly polarized light passes through the first layer, it is transmitted to the second layer as elliptically polarized light as a result of interaction with the linear optical anisotropy of the layer. The molecules of the second layer, upon absorbing the light transmitted from the previous layer, reorient so their transition dipole moments are perpendicular to the long axis of the polarization ellipse. This in turn changes the azimuth of the polarization transmitted to the next layer. Overall the effect is a type of self-rotation of the light by the mesogens, and mesogens by the light. This process is illustrated schematically in Figure 1. The authors also study a liquid-crystalline polymer in the same paper, but conclude that it does not obey the polarization propagation model as well. They suggest that perhaps the existence of domains with random orientation causes the creation of many parallel helices, wound in the same sense but with different starting orientations. It was postulated that this may affect the light propagation in a way analogous to classical optical activity in solutions.

Recently Kim et al. have reported photoinduced circular anisotropy in an amorphous epoxy-based azo polymer by elliptically polarized light.[36] Using a commericial CD spectrophotometer they have acquired CD spectra at various stages of irradiation. They attribute the changes in shape and position of the CD bands to a change in the association of azo chromophores from parallel alignment (resulting in a spectral blue-shift) to an in-line alignment (red-shift). This is in accordance with Kasha's exciton model[37] for electronic transitions in molecular aggregates.

Rather than allowing the azo polymer to develop a pitch which may involve many experimental and material factors, an interesting experiment has been performed by Birabassov and Galstian[38] in which two counter-propagating circularly polarized beams were used to set up a helicoidal standing wave. Such an electromagnetic field has uniform intensity but varying polarization along the propagation axis. A cellulose acetate film doped with the azo dye DR1 was irradiated with this beam, but no optical activity was observed. Subsequent calculations performed by the authors using de Vries' equation[15] show that the anticipated optical rotation is below their detection limit.

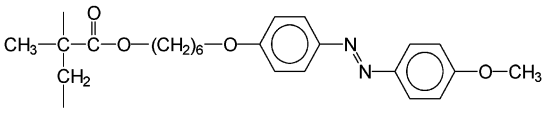

$G$ 75°C $S_A$ 95°C $N$ 135°C $I$

**Figure 2.** Molecular structure and phase sequence of the liquid-crystalline azo polymer pMAB6.

A study by Ichimura and Han[39] reported photoinduced chirality in a liquid-crystalline azo polymer exposed to sunlight. Films were placed outdoors and, as the sun travelled across the sky over a period of hours, the in-plane dichroism of the films was periodically monitored. The orientation of the mesogens was along the propagation direction of the light, which changed in polar and azimuthal angle as the sun rose and set.

In this report we investigate these photoinduced helices in a liquid-crystalline azo polymer. First, we will describe the material we are studying (section 2) and provide the relevant details on the preparation of the sample. Next, in section 3, we will describe the experiments that were performed; there are two types. In the first experiment the pump beam is switched between left-circularly polarized (LCP) and right-circularly polarized (RCP) 14 times (7 LCP−RCP cycles) while irradiating the same spot on a film of the liquid-crystalline polymer pMAB6. In the second experiment, the handedness of the pump beam is fixed as LCP and the film is exposed in small doses so the evolution of the anisotropy may be monitored; this is then repeated for a RCP pump. Section 4 will introduce and describe the formalism for the models that were used to treat the experimental data. We wish to emphasize that our modeling does not provide complementary information but is required to interpret the data and make connections to the orientation of the azo chromophores on a microscopic level. (For the reader less interested in the details of these models, it is possible to skip section 4.) The results of the experiments, obtained by treating the measured polarization data with the models, are described in section 5. Here, a uniaxial model of the resulting anisotropy is used to fit the data from both experiments. Then, a more structural model that explicitly describes helical ordering is used to treat data from the second experiment. Finally the general discussion (section 6) aims to interpret these results and make inferences on key issues in the broader topic of photoinduced chirality in azo materials.

## 2. Material and Sample Preparation

The material used in this study, named pMAB6, is a liquid-crystalline azo polymer and was prepared for us in a manner similar to that described in refs 40 and 41; its structure and phase sequence are shown in Figure 2. Films of the polymer were spin cast from a tetrahydrofuran solution onto clean glass slides with no surface preparation. Freshly prepared films were amorphous, but the ones used in these studies were first annealed by heating to 140 °C and then cooling to room temperature, thereby trapping the nematic phase. The material has a number-average molecular weight of 27 000 g/mol and a polydispersity index of 2.1. Further details about the sample preparation and phase characterization may be found in Ref 42. Thickness measurements were obtained using a Sloan Dektak IIA profilometer.

### 3. Description of the Experiments

The first experiments that were performed exposed a thick film ($d = 3.88$ $\mu$m) of pMAB6 to alternating cycles of left-circularly polarized and right-circularly polarized light from an $Ar^+$ laser ($\lambda = 488$ nm) with $I = 70$ mW/cm$^2$ in 14 intervals of 30 min each, with the exception of the first irradiation which was for 20 min. After a 1-min relaxation period following each exposure, the sample was rotated about the lab *y*-axis (vertical) so that a red HeNe ($\lambda = 632.8$ nm) probe beam (irradiance $5 \times 10^{-2}$ mW/cm$^{-2}$) met with the addressed area of the sample at normal incidence. This probe beam was linearly polarized, and its azimuth was stepped through the angles $0° \leq \beta \leq 360°$ in 10° increments. The transmitted light was analyzed with a homemade single-wavelength single-detector Stokes polarimeter that provided the Stokes parameters ($S_0$, $S_1$, $S_2$, and $S_3$) as a function of $\beta$. Detailed information about the polarimeter setup and data acquisition appear in our previous publication.[43]

In a second set of experiments, a 3.95-$\mu$m sample of pMAB6 was irradiated with LCP light from the same $Ar^+$ laser with $I = 70$ mW/cm$^2$ in intervals of 5 min, followed by a 1-min relaxation period, for a total time of ca. 3.5 h. The same polarization analysis at $\lambda = 632.8$ nm followed, collecting $S_j(\beta)$. The pump beam polarization was then switched to RCP and the experiment was repeated on a new spot on the film.

In the sign conventions used here, propagation is along the positive *z*-axis as $\mathbf{E} = \mathbf{E}_0\, e^{kz-i\omega t}$. In this case, right-handed polarization states are characterized by $\Delta\phi \equiv \phi_y - \phi_x < 0$ and correspondingly negative ellipticities. This convention is illustrated in Figure 3a and b.

### 4. Formalism: Models that Relate the Polarization Change to the Optical Constants

As the azimuth of the probe beam is varied through $0° \leq \beta \leq 360°$, the incident field may be described by the Jones vector

$$E_{in} = \begin{bmatrix} \cos\beta \\ \sin\beta \end{bmatrix} \tag{1}$$

Two models will be considered below, and the goal for each of them is to arrive at an expression for the transmitted field $E_{out}$ in terms of the anisotropic optical constants that serve as order parameters in the models. The polarization of the output field is then obtained using

$$S_0 = E_x E_x^* + E_y E_y^*$$

$$S_1 = E_x E_x^* - E_y E_y^*$$

$$S_2 = E_x E_y^* + E_y E_x^*$$

$$S_3 = i(E_x E_y^* - E_y E_x^*) \tag{2}$$

where $E_x$ and $E_y$ are the *x*- and *y*-components of the output field, and the asterisk denotes the complex conjugate. These Stokes parameters may be compared with those measured experimentally using the polarimeter. Working in the reverse order, fitting the polarization data to one of the models below affords the anisotropic optical constants. Further details of the fitting process are included in ref 43.

**4.1. Model 1: Uniaxial Model.** Helical structures interact with polarized light in a manner that displays both linear and circular anisotropy. The first model that is considered is one in which the linear anisotropy describes a uniaxial arrangement with three order parameters: (1) the linear dichroism $\Delta\alpha_{lin} \equiv \alpha_y - \alpha_x$, (2) linear birefringence $\Delta n_{lin} \equiv n_y - n_x$, and (3) the orientation of the slow axis $\theta$. The circular anisotropy is included on a phenomenological level only, that is, without any structural interpretation. This introduces the final two order parameters corresponding to (4) the circular dichroism $\Delta\alpha_{cir} \equiv \alpha_{left} - \alpha_{right}$ and (5) circular birefringence $\Delta n_{cir} \equiv n_{left} - n_{right}$. While it seems natural to describe the dichroism in terms of the difference in absorption coefficients, since we are following the electric component of the optical field through the sample, it is more practical to work with the field attenuation coefficients $\kappa_{x,y}$, which are the imaginary components of the complex refractive index. These are related as

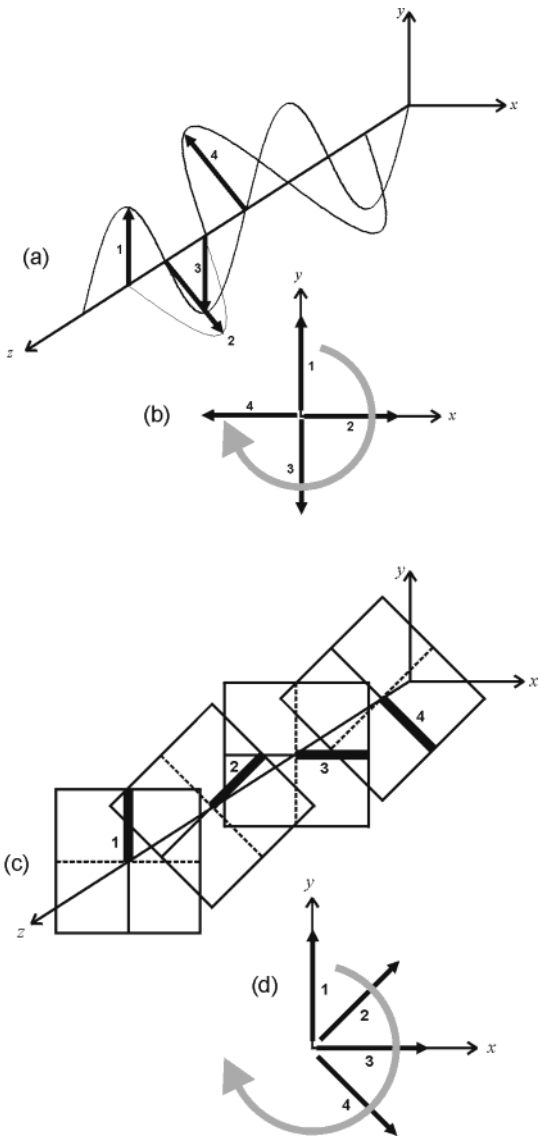


**Figure 3.** Snapshot of right-circularly polarized light frozen in time showing (a) *x*- and *y*-components of **E** and (b) the convention used to determine the handedness of the polarization. (c) The handedness of a helix is assigned using a similar convention, resulting in (d) the determination of a right-handed structure.

$$\Delta\alpha = \frac{2k_0}{\ln 10}\Delta\kappa \tag{3}$$

where $k_0 = 2\pi/\lambda_0$.

A polarization transfer operator, *T*, has been constructed using Jones calculus[44] which incorporates these five parameters. Details of this model have been provided previously,[43] so only the final results will be summarized here. The goal is to arrive

at the output field using

$$E_{out} = TE_{in} \tag{4}$$

The transfer operator is obtained from

$$T = R(-\theta)t_{back}S_{\infty}Mt_{front}R(\theta) \tag{5}$$

where $R(\theta)$ performs a rotation from the laboratory $xy$ frame through an angle $\theta$ to the slow−fast axes of the sample, and $t_{front}$ and $t_{back}$ are operators that account for the Fresnel transmission coefficients for crossing the air-film and film−substrate interfaces. A single pass through the sample is achieved by

$$M = \begin{bmatrix} -\frac{1}{2\xi}ik_0d\Delta N_{lin}\sin\xi + \cos\xi & \frac{1}{2\xi}k_0d\Delta N_{cir}\sin\xi \\ -\frac{1}{2\xi}k_0d\Delta N_{cir}\sin\xi & \frac{1}{2\xi}ik_0d\Delta N_{lin}\sin\xi + \cos\xi \end{bmatrix} e^{ik_0Nd} \tag{6}$$

where the material parameters are contained in $\Delta N_{lin} \equiv \Delta n_{lin} + i\Delta\kappa_{lin}$ and $\Delta N_{cir} \equiv \Delta n_{cir} + i\Delta\kappa_{cir}$, $d$ is the film thickness, and $\xi \equiv 1/2k_0d\sqrt{\Delta N_{lin}{}^2+\Delta N_{cir}{}^2}$. The effects of thin-film interference are taken into account by considering an infinite amount of passes by reflection inside the sample, thus

$$S_{\infty} = \frac{1}{1 - Mr_{front}Mr_{back}} \tag{7}$$

with the Fresnel reflection coefficients contained in the reflection operators $r_{front}$ and $r_{back}$.

**4.2. Model 2: Twisted-Stack Model.** This model describes the film as a series of stacked layers, each containing only linear anisotropy and with its optical axis twisted with respect to the previous layer, thereby forming a helix. There should therefore be four order parameters: (1) the birefringence and (2) dichroism within a layer, (3) the pitch, and (4) the orientation of the optical axis at the input face (air−film interface).

The first obstacle encountered is that Jones calculus may not be used to described the change in polarization state of the probe beam upon traversing such a helix. This is because it is not possible to rotate the coordinate system so that the axis of the film's anisotropy coincides with one of the basis vectors of the laboratory reference frame since the optical axis is rotating layer-by-layer. In this case it is necessary to resort to a more complete level of theory in which the entire electromagnetic wave (considering **E** and **H**) propagates through the sample. There are several schemes for dealing with light propagation through stratified media in general[45] and helices in particular, including an extension of Jones calculus,[46] a unique 2 × 2 matrix method,[47] Berreman's 4 × 4 matrix technique,[48,49] and a formalism in terms of the complex polarization developed by Azzam and Bashara.[50−52] The current treatment will follow the method of Berreman developed for oblique incidence,[53] but for the simplier case of normal incidence, parallel to the helical axis.

We want to represent the linear anisotropy with the order parameters $\Delta\alpha$ (or $\Delta\kappa$) and $\Delta n$ but express them in terms of $\Delta\epsilon$ in this model. Since $\epsilon = (n + i\kappa)^2$, the required anisotropy is described by

$$\Delta\epsilon \equiv \epsilon_y - \epsilon_x = 2(n_{iso} + i\kappa_{iso})(\Delta n + i\Delta\kappa) \tag{8}$$

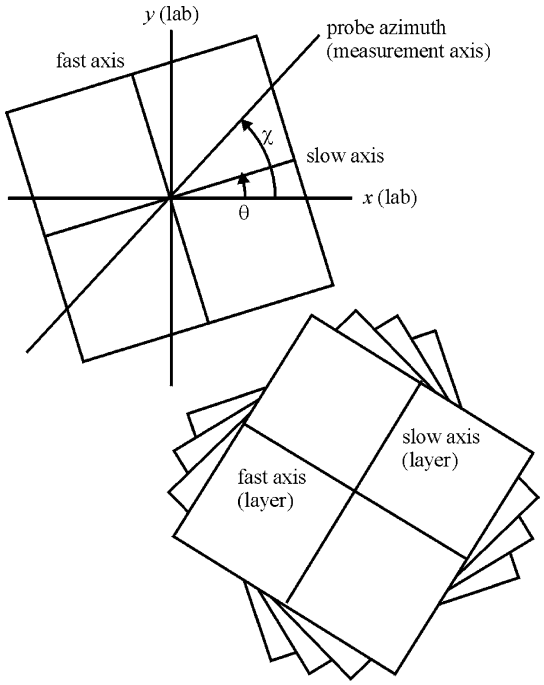


**Figure 4.** In the twisted-stack model, the sample thickness is divided into layers, each described only by its linear anisotropy and orientation of the optical axis. The optical axis rotates from layer-to-layer, forming the helix with a characteristic pitch.

Interest in such twisted materials has been strong since the discovery of cholesteric liquid crystals, and much of the theory of the optical properties of macroscopic helices has been developed for that purpose. The simplest model, proposed by Oseen,[54] simply rotates the components of the dielectric tensor so

$$\epsilon = \begin{bmatrix} \bar{\epsilon} & 0 & 0 \\ 0 & \bar{\epsilon} & 0 \\ 0 & 0 & \epsilon_z \end{bmatrix} - \frac{\Delta\epsilon}{2}\begin{bmatrix} -\frac{\Delta\epsilon}{2} & 0 & 0 \\ 0 & \frac{\Delta\epsilon}{2} & 0 \\ 0 & 0 & 0 \end{bmatrix}\begin{bmatrix} \cos 2\chi & \sin 2\chi & 0 \\ -\sin 2\chi & \cos 2\chi & 0 \\ 0 & 0 & 0 \end{bmatrix} \tag{9}$$

where $\bar{\epsilon} = 1/2(\epsilon_x + \epsilon_y)$ and $\chi$ is the azimuth of the current layer with respect to the laboratory $x$-axis. The rotation is performed with periodicity $2\chi$ since the structure repeats itself after a distance equal to half the pitch, rather than the full pitch. This is a consequence of indistinguishable parallel and antiparallel orientations of the molecules/optical axes. Oseen considers the director at the entrance face of the helix ($z = 0$, the air−film interface) to be along the $x$-axis. We wish to consider that the helix may be wound starting with an arbitrary initial azimuth $\gamma_{initial}$, thereby allowing one additional degree of freedom. Here $\gamma$ is the orientation of the fast axis within a layer, so $\theta = \gamma - 90°$. Therefore,

$$\chi = \gamma_{initial} + \frac{2\pi z}{P} \tag{10}$$

where $P$ is the pitch and $z$ is the distance along the film from $z = 0$ at the air−film interface to $z = d$ at the film−glass interface. With this convention, a right-handed helix−one in which the director rotates in a clockwise manner−is described by $P < 0$, just as RCP light is characterized by $\Delta\phi < 0$ (see Figure 3). For simplicity, let $\bar{\epsilon} = \epsilon_z = \epsilon_{iso}$. A few such layers in the stack are illustrated in Figure 4.

Consider a wave traveling along the helical axis $\hat{z}$ as $\psi(z)e^{-i\omega t}$ where

$$\psi = \begin{bmatrix} E_x \\ H_x \\ E_y \\ H_y \end{bmatrix} \tag{11}$$

Expanding Maxwell's relation

$$\nabla \times \mathbf{E} = -\frac{\partial \mathbf{B}}{\partial t} \tag{12}$$

and using

$$\mathbf{B} = \mu \mathbf{H} \tag{13}$$

together with the approximation $\mu = \mu_0\mu_\mathbf{r} \approx \mu_0$ (for nonmagnetic materials) as

$$\begin{bmatrix} \partial/\partial x \\ \partial/\partial y \\ \partial/\partial z \end{bmatrix} \times \begin{bmatrix} E_x \\ E_y \\ E_z \end{bmatrix} = -\mu_0 \frac{\partial}{\partial t} \begin{bmatrix} H_x \\ H_y \\ H_z \end{bmatrix} \tag{14}$$

results in the relations

$$\begin{aligned} \frac{\partial E_y}{\partial z} &= -i\omega\mu_0 H_x \\ \frac{\partial E_x}{\partial z} &= i\omega\mu_0 H_y \\ H_z &= 0 \end{aligned} \tag{15}$$

since $\partial\psi/\partial x = \partial\psi/\partial y = 0$. Next consider

$$\nabla \times \mathbf{H} = \frac{\partial \mathbf{D}}{\partial t} \tag{16}$$

along with

$$\mathbf{D} = \epsilon \mathbf{E} \tag{17}$$

where $\epsilon = \epsilon_0\epsilon_\mathbf{r}$. This may be expanded in the form

$$\begin{bmatrix} \partial/\partial x \\ \partial/\partial y \\ \partial/\partial z \end{bmatrix} \times \begin{bmatrix} H_x \\ H_y \\ H_z \end{bmatrix} = \epsilon_0 \begin{bmatrix} \epsilon_{xx} & \epsilon_{xy} & \epsilon_{xx} \\ \epsilon_{yx} & \epsilon_{yy} & \epsilon_{yz} \\ \epsilon_{zx} & \epsilon_{zy} & \epsilon_{zz} \end{bmatrix} \frac{\partial}{\partial t} \begin{bmatrix} H_x \\ H_y \\ H_z \end{bmatrix} \tag{18}$$

to yield the relations

$$\begin{aligned} \frac{\partial H_y}{\partial z} &= i\omega\epsilon_0(\epsilon_{xx}E_x + \epsilon_{xy}E_y + \epsilon_{xz}E_z) \\ \frac{\partial H_x}{\partial z} &= -i\omega\epsilon_0(\epsilon_{yx}E_x + \epsilon_{yy}E_y + \epsilon_{yz}E_z) \\ 0 &= -i\omega\epsilon_0(\epsilon_{zx}E_x + \epsilon_{zy}E_y + \epsilon_{zz}E_z) \end{aligned} \tag{19}$$

The last of the above relations may be solved for $E_z$, which may then be used to eliminate $E_z$ from the other equations. Finally this results in a set of four equations:

$$\begin{aligned} \frac{\partial E_x}{\partial z} &= i\omega\mu_0 H_y \\ \frac{\partial H_x}{\partial z} &= -i\omega\epsilon_0\left(\epsilon_{xx} - \frac{\epsilon_{xz}\epsilon_{zx}}{\epsilon_{zz}}\right)E_x + i\omega\epsilon_0\left(\epsilon_{xy} - \frac{\epsilon_{xz}\epsilon_{zy}}{\epsilon_{zz}}\right)E_y \\ \frac{\partial E_y}{\partial z} &= -i\omega\mu_0 H_x \\ \frac{\partial H_y}{\partial z} &= i\omega\epsilon_0\left(\epsilon_{yz} - \frac{\epsilon_{yz}\epsilon_{zx}}{\epsilon_{zz}}\right)E_x - i\omega\epsilon_0\left(\epsilon_{yz} - \frac{\epsilon_{yz}\epsilon_{zy}}{\epsilon_{zz}}\right)E_y \end{aligned} \tag{20}$$

It has been shown that for a wave traveling parallel to the helical axis ($\hat{z}$), Maxwell's relations may be written in the form

$$\frac{\partial}{\partial z}\psi(z) = \mathbf{D}(z)\psi(z) \tag{21}$$

where $\mathbf{D}(z)$ is a matrix form of the right-hand side of Equations 20 written here as

$$\mathbf{D}(z) = i\omega \begin{bmatrix} 0 & 0 & 0 & \mu_0 \\ \epsilon_0\epsilon_{yz}\epsilon_{xx}/\epsilon_{zz} - \epsilon_0\epsilon_{yx} & 0 & -\epsilon_0\epsilon_{yy} + \epsilon_0\epsilon_{yz}\epsilon_{zy}/\epsilon_{zz} & 0 \\ 0 & \mu_0 & 0 & 0 \\ \epsilon_0\epsilon_{xx} - \epsilon_0\epsilon_{xx}\epsilon_{xx}/\epsilon_{zz} & 0 & \epsilon_0\epsilon_{xy} - \epsilon_0\epsilon_{xx}\epsilon_{zy}/\epsilon_{zz} & 0 \end{bmatrix} \tag{22}$$

The solution of this equation for propagation over some small distance $h$ is

$$\psi(z + h) = e^{\mathbf{D}(z)h}\psi(z) \tag{23}$$

since it is assumed that $\mathbf{D}$ is constant if $h \ll P$. The local propagation operator $\mathbf{P}(z, h)$ is defined by the matrix exponential

$$\mathbf{P}(z, h) \equiv e^{D(z)h} = \sum_{n=0}^{\infty} \frac{[\mathbf{D}(z)]^n h^n}{n!} \tag{24}$$

so

$$\psi(z + h) = \mathbf{P}(z, h)\psi(z) \tag{25}$$

To describe the helix, the film is divided into $m$ layers so $h = d/m$. For a macroscopic distance such as the entire film thickness $d$, one must solve

$$\psi(z + d) = \mathbf{F}(z, d)\psi(z) \tag{26}$$

where

$$\mathbf{F}(z, d) = \prod_m \mathbf{P}(z, h) \tag{27}$$

Once the macroscopic propagation operator $\mathbf{F}(z, d)$ has been determined, it may be used to get the light through the film from $z = 0$ to $z = d$, thus solving for the propagation through the helix.

Eq 26 may be realized in Figure 5 where it is seen that the wave on the air side of the film at $z = 0$ has an incident component $\psi^i$ and a reflected component $\psi^r$. The transmitted wave $\psi^t$ is found on the glass side of the film at $z = d$. The formalism developed so far allows $\mathbf{F}$ to be written in terms of the sought order parameters $\Delta n_{\text{layer}}$, $\Delta\alpha_{\text{layer}}$, $P$, and $\gamma_{\text{initial}}$. Now, knowing $\psi^i$ that is sent toward the sample, the goal is to solve

$$\psi^t = \mathbf{F}(\psi^i + \psi^r) \tag{28}$$

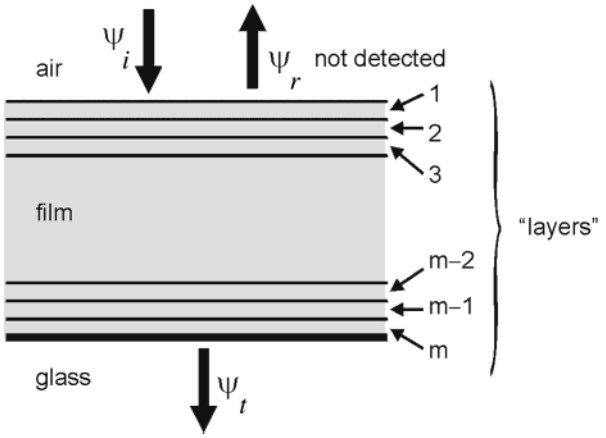


**Figure 5.** After constructing the general propagation matrix **F**, the reflected and transmitted waves may be obtained if the incident wave is known.

Making use of the relation between **E** and **H** for the incident light

$$\mathbf{H} = \sqrt{\frac{\epsilon_0}{\mu_0}} n \mathbf{k}_0 \times \mathbf{E} \tag{29}$$

results in

$$H_x^i = -\sqrt{\frac{\epsilon_0 \epsilon_r}{\mu_0}} E_y^i$$

$$H_y^i = \sqrt{\frac{\epsilon_0 \epsilon_r}{\mu_0}} E_x^i \tag{30}$$

(with an analogous set of relations for the transmitted wave) and also

$$H_x^r = \sqrt{\frac{\epsilon_0 \epsilon_r}{\mu_0}} E_y^r$$

$$H_y^r = -\sqrt{\frac{\epsilon_0 \epsilon_r}{\mu_0}} E_x^r \tag{31}$$

for the reflected wave, the problem may be stated in terms of the electric components only, from which the polarization information is obtained. Now the problem appears as

$$\begin{bmatrix} E_x^t \\ -\sqrt{\epsilon_0 \epsilon_r / \mu_0} E_y^t \\ E_y^t \\ \sqrt{\epsilon_0 \epsilon_r / \mu_0} E_x^t \end{bmatrix} = \mathbf{F} \begin{bmatrix} E_x^i + E_x^r \\ -\sqrt{\epsilon_0 \epsilon_r / \mu_0} E_y^i + \sqrt{\epsilon_0 \epsilon_r / \mu_0} E_y^r \\ E_y^i + E_y^r \\ \sqrt{\epsilon_0 \epsilon_r / \mu_0} E_x^i + \sqrt{\epsilon_0 \epsilon_r / \mu_0} E_x^r \end{bmatrix} \tag{32}$$

which is a system of four equations in four unknowns. Since the reflected beam is not detected in the geometry of the experiment, the only variables of interest are $E_x^t$ and $E_y^t$. These are then converted into a Stokes vector description of the polarization using eq 2. It is now possible to model the Stokes polarimetry experiment for an arbitrary helical structure whose axis is normal to the film surface and parallel to the propagation vector of the probe beam.

Figure 6 shows the polarization data (symbols) collected for a film exposed to RCP light for 210 min. The lines are drawn from fitting results obtained using this twisted stack model with

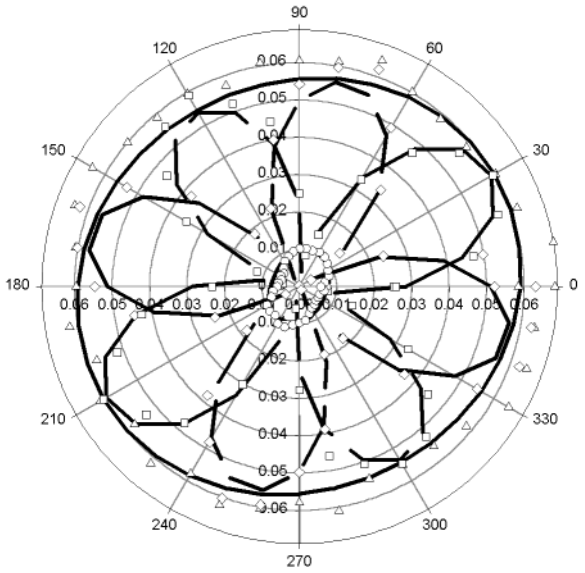


**Figure 6.** Sample polarimetry data showing the Stokes parameters $S_j$ measured as a function of the probe beam azimuth $\beta$ for 210 min irradiation with right-circularly polarized light. The experimental data is shown with the symbols △ $S_0$, ◇ $S_1$, □ $S_2$, and ○ $S_3$. Curves are drawn from the twisted-stack model fitting results (negative values are indicated with dashed lines) with $\Delta n_{layer} = 0.137$, $\Delta\alpha_{layer} = 0.192\ \mu m^{-1}$, $P = 1594$ nm, and $\gamma_{initial} = 1.1°$.

$\Delta n_{layer} = 0.137$, $\Delta\alpha_{layer} = 0.192\ \mu m^{-1}$, $P = 1594$ nm, and $\gamma_{initial} = 1.1°$ (dashed lines indicate negative values).

## 5. Results

**5.1. Data from the Switching Experiment Treated with the Uniaxial Model.** When the uniaxial model was applied to all 14 data sets in the switching experiment, the resulting order parameters are shown in Figures 7 and 8. The success of the present phenomenological model in accounting for the circular anisotropy induced by the CP light may best be seen in Figure 7 where the results of the $\Delta\alpha_{cir}$ and $\Delta n_{cir}$ determination are shown. The experiments are numbered starting with the first set of LCP exposure (expt 1) followed by RCP exposure (expt 2), then LCP again (expt 3), and RCP (expt 4) until the seventh cycle of LCP (expt 13) and RCP (expt 14) is completed. It may be seen that in all cases irradiation with LCP light results in $\Delta\alpha_{cir} < 0$ and $\Delta n_{cir} < 0$ (laevorotatory behavior). Irradiation with RCP light then induces $\Delta\alpha_{cir} > 0$ and $\Delta n_{cir} > 0$ (dextrarotatory behavior). It is interesting to see that the magnitude of the anisotropy is equal with opposite sign for each LCP−RCP cycle. To achieve this, the initial LCP exposure was 20 min long, followed by a 30 min RCP irradiation. The magnitude of the anisotropy decreases with each cycle, seen most clearly in the case of the circular birefringence. A likely explanation is that the first exposure created an initial helical structure from a random orientation of mesogens, while the second exposure with light of opposite handedness first had to 'unwind' the existing helix, then reinscribe one with the opposite handedness. That the magnitude of the anisotropy decreases with each subsequent irradiation period is very likely the result of an increasing homeotropic alignment as mesogens tend parallel to the light propagation direction, normal to the film surface. This explanation has already been suggested by Iftime et al.[29] for a similar switching experiment that was monitored using a commercial CD spectrophotometer. Further, this polymer has already been reported in the literature to have a facile in-plane to out-of-plane reorientation with either linearly-polarized or unpolarized irradiation.[55−58]

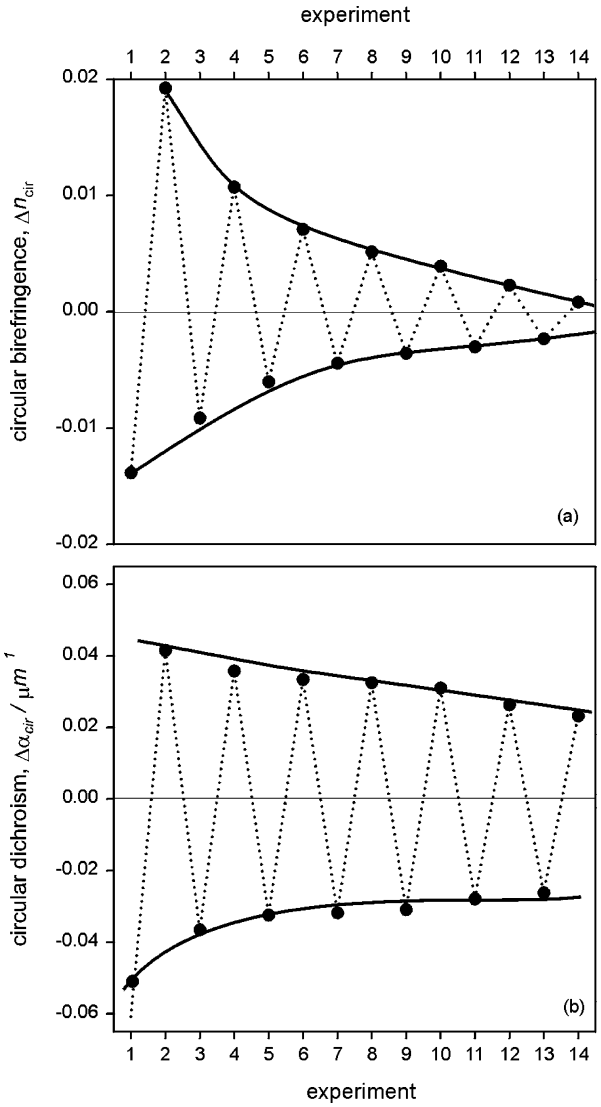


**Figure 7.** Results of (a) circular birefringence and (b) dichroism obtained by fitting the phenomenological model to the data obtained in the switching experiments. Experiment 1 consisted of LCP irradiation for 20 min. Subsequent odd-numbered experiments 3−13 indicate exposure to LCP light for 30 min; even-numbered experiments 2−14 correspond to 30 min of RCP light.

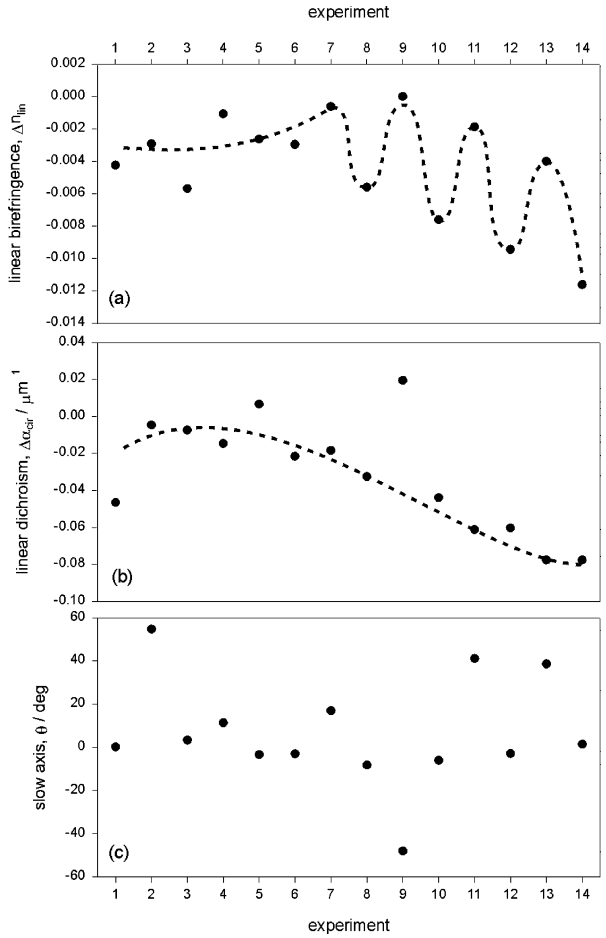


**Figure 8.** Results of (a) linear birefringence and (b) dichroism, along with (c) the orientation of the corresponding slow axis, obtained by fitting the phenomenological model to the data obtained in the switching experiments. Odd-numbered experiments 1−13 indicate exposure to LCP light for 30 min; even-numbered experiments 2−14 correspond to 30 min of RCP light.

The remaining three parameters corresponding to the linear anisotropy ($\Delta\alpha_{lin}$, $\Delta n_{lin}$ and $\theta$) are shown in Figure 8. The linear birefringence shows a zigzag dependence on the pump polarization, with larger values occurring for RCP light. There is a small pump handedness-dependence for the linear dichroism as well, but the results are not as clear. Finally, the orientation of the slow axis appears quite random over a large range. Since the linear anisotropy results from a helical arrangement of mesogens, scattered results are somewhat expected since the winding and unwinding of the helical structures creates new structures for every experiment−the only anticipated trend should be in the circular anisotropy and this is what is observed. Although it is difficult to interpret the information that comes from the determination of the linear order parameters in such an experiment, what is important is that the linear parameters are separated from the sought circular ones, so the true circular dichroism and birefringence may be obtained.

**5.2. Data from the Stepwise Irradiation Experiment Treated with the Uniaxial Model.** A 3.95-$\mu$m sample of pMAB6 was irradiated with LCP light from the same $Ar^+$ laser at 70 mW/cm$^2$ in intervals of 5 min. When the resulting $S_j(\beta)$ data were fit to the present model, the five corresponding order parameters ($\Delta\alpha_{cir}$, $\Delta n_{cir}$, $\Delta\alpha_{lin}$, $\Delta n_{lin}$, $\theta$) were obtained; results of circular anisotropy determination are shown in Figure 9a. Here it is seen that upon the onset of the irradiation, the circular birefringence and dichroism both tend in the negative direction, reaching their maximum values near 45 min exposure. Comparing these values with the ones obtained during the switching experiment shows that at 30 min the same level of anisotropy is observed. Since repeated switching cycles resulted in a decrease in the level of anisotropy in the circular constants, it was hypothesized that prolonged exposure with a fixed handedness would also eventually reduce the levels of $\Delta\alpha_{cir}$ and $\Delta n_{cir}$. Initially this was observed since, after 45 min exposure, the values of these constants began to decrease, tending toward zero. Keeping the pump on for a prolonged period afterward, we were astonished to see the levels of $\Delta\alpha_{cir}$ and $\Delta n_{cir}$ begin to increase again, but this time in the opposite direction. Finally, after ca. 3 h, the constants approached a stable value and leveled off with positive values. The two curves cross zero at different times, with $\Delta\alpha_{cir}$ making the first crossing at about 1.2 h, followed by $\Delta n_{cir}$ at about 2.1 h after the start of the experiment. The order parameters corresponding to the linear anisotropy are shown in Figure 9b where it is seen that the linear dichroism and birefringence both go through a maximum. It is interesting to note that $\Delta\alpha_{lin}$ and $\Delta n_{lin}$ have almost the same behavior here. Looking at the evolution of the optical axis in Figure 9c, there is a steady linear decrease and then a sudden drop at around

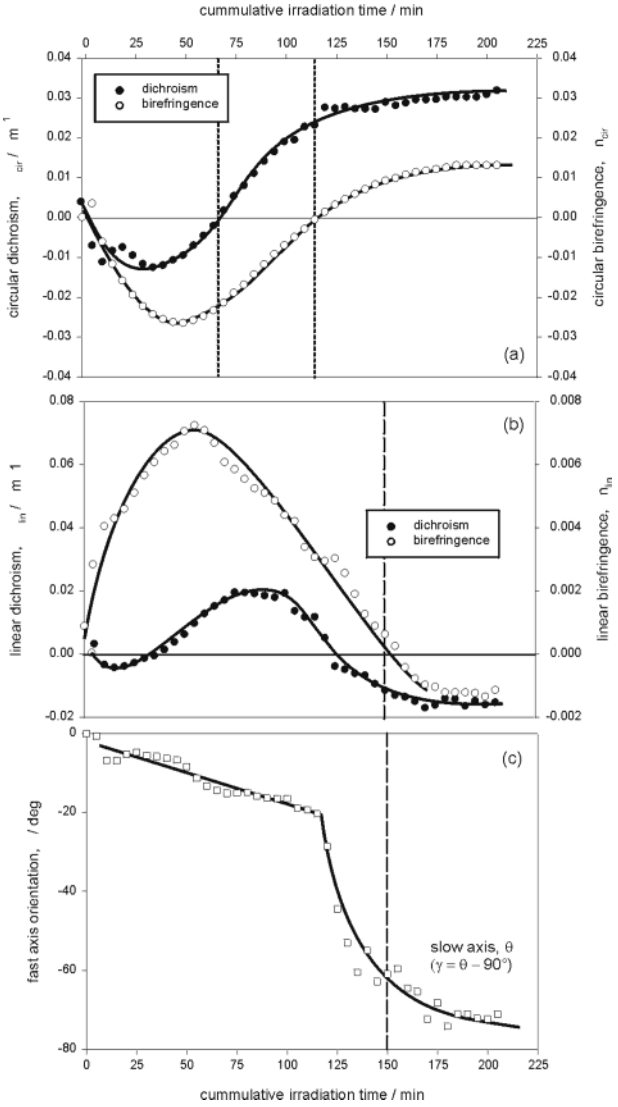


**Figure 9.** Results of circular and linear anisotropy determination using the uniaxial model when the LC sample was exposed to LCP light for intervals of 5 min. (a) Shows the circular dichroism and birefringence, (b) the linear dichroism and birefringence, and (c) the evolution of the fast axis.

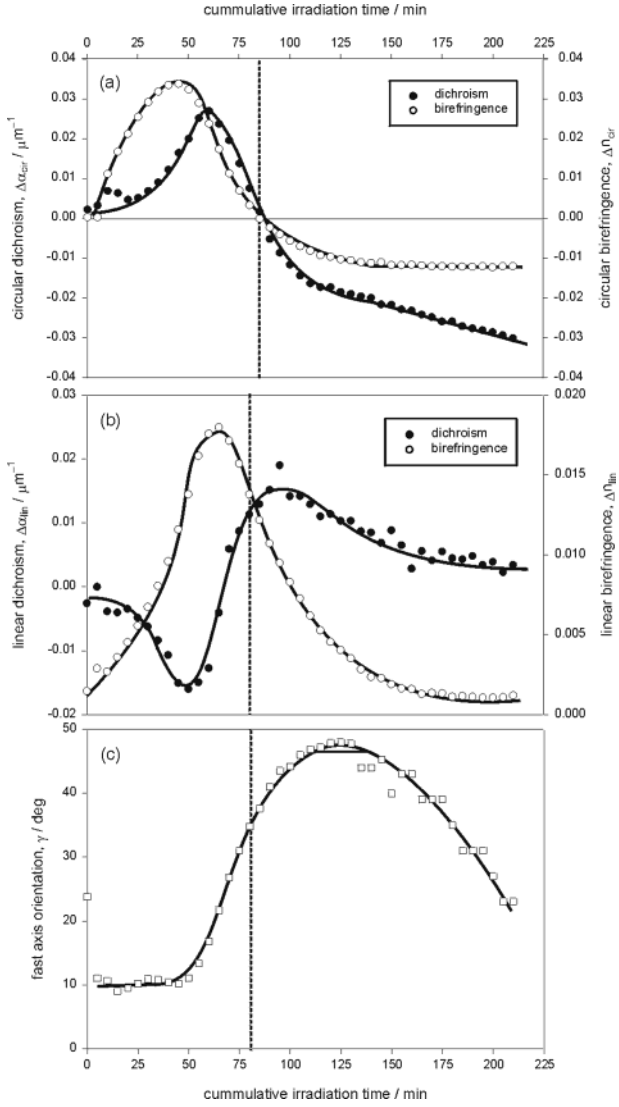


**Figure 10.** Results of circular and linear anisotropy determination using the uniaxial model when the LC sample was exposed to RCP light for intervals of 5 min. (a) Shows the circular dichroism and birefringence, (b) the linear dichroism and birefringence, and (c) the evolution of the fast axis.

**TABLE 1: Conventions for Changing the Signs of the Order Parameters Describing the Linear Anisotropy and the Corresponding Orientations of the Optical Axes**

| $\Delta\alpha_{lin}$, $\Delta n_{lin}$ | slow axis | fast axis |
|---|---|---|
| $- \rightarrow +$ | $\theta \rightarrow \theta + 90°$ | $\gamma \rightarrow \gamma - 90°$ |
| $+ \rightarrow -$ | $\theta \rightarrow \theta - 90°$ | $\gamma \rightarrow \gamma + 90°$ |

115 min. Since the linear dichroism and birefringence are both represented by negative values in this region, the optical axis is actually shifted down by an additional 90° here. Conventions which describe whether the axis should be shifted up or down depending on the sign of the linear anisotropy are listed in Table 1.

The experiment was then repeated on a new spot on the same sample, but this time with RCP light. Results of circular anistropy determination are shown in Figure 10a. Here the profiles of $\Delta\alpha_{cir}$ and $\Delta n_{cir}$ are flipped with respect to those obtained for the LCP light. A marked difference, however, is that $\Delta\alpha_{cir}$ and $\Delta n_{cir}$ now cross zero at exactly the same point, just before 1.5 h of irradiation. Examining the order parameters corresponding to the linear anisotropy shown in Figure 10b, it is seen that the linear dichroism and birefringence have the same profile as that obtained for the experiment with the LCP light. Although the features are sharper here and the birefringence is more peaked, the maximum values in $\Delta n_{lin}$ occur around 1 h exposure for both LCP and RCP irradiation. The optical axis progression shown in Figure 10c displays the opposite behavior, indicating that twisting occurred in the opposite direction.

**5.3. Data from the Stepwise Irradiation Experiment Treated with the Twisted-Stack Model.** The data from the switching experiment were not treated with this model since it was anticipated that the structures induced with the alternating LCP−RCP cycles would be new in each case. With no opportunity to observe a trend in the order parameters, there would be no indication of whether the results of such fitting are reasonable or not. For this reason, the twisted-stack model considered here was used to fit the data from the stepwise irradiation experiment only. After some preliminary test fits to determine the ranges of the parameters, the helical structures were considered to consist of 100 layers. If fewer than 100 layers were used for the calculation, the results would be sensitive to the number of layers. This is because the distance $h$ in the propagation model then becomes too large and eq 23 is no longer valid. When more than 100 layers are used in the

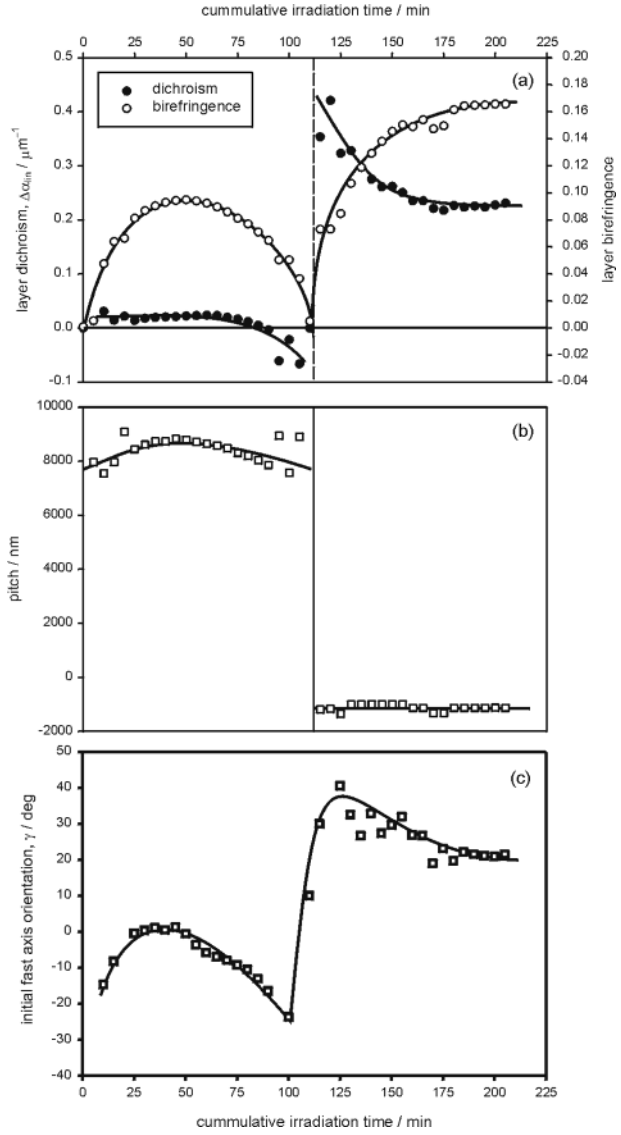


**Figure 11.** Results of the stepwise irradiation experiment with LCP from fitting to the twisted-stack model, showing (a) the linear dichroism and birefringence per layer, (b) the pitch, and (c) the initial orientation of the fast axis.

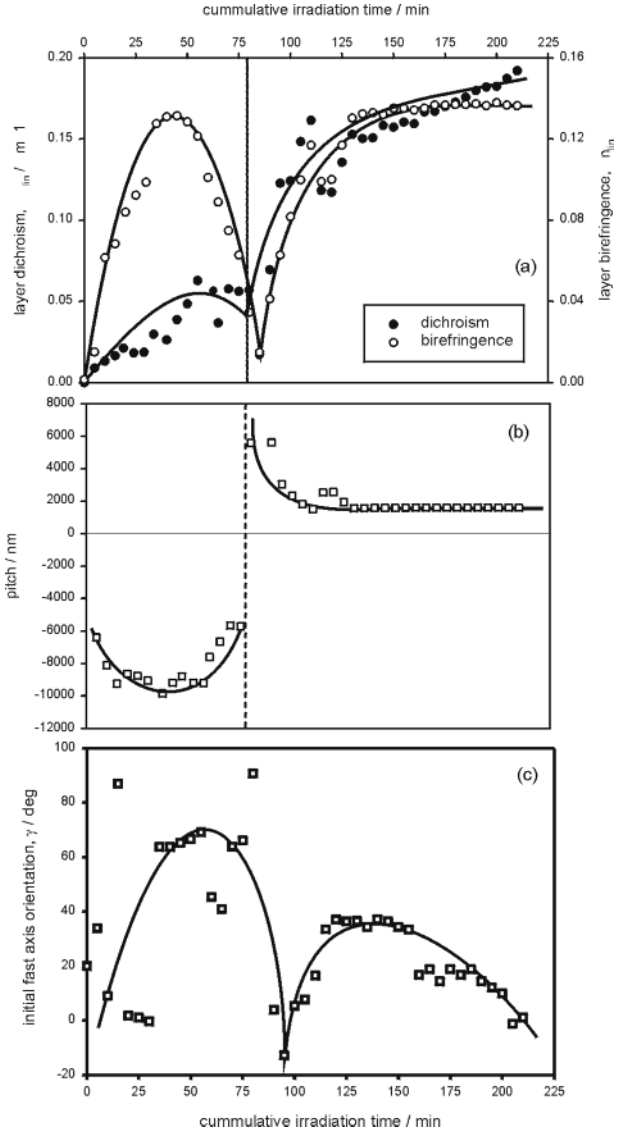


**Figure 12.** Results of the stepwise irradiation experiment with RCP from fitting to the twisted-stack model, showing (a) the linear dichroism and birefringence per layer, (b) the pitch, and (c) the initial orientation of the fast axis.

calculation, the results are not significantly affected but the computation time increases considerably. Figure 11 shows the results for (a) the per-layer dichroism and birefringence and (b) pitch determination when irradiation was performed with a LCP pump. Examining these plots together, there is a common discontinuity at 110 min of irradiation. This is most evident in the pitch determination, where the pitch changes sign from positive to negative. Before this time, there is a near-constant, very small amount of dichroism per layer, while the birefringence goes through a maximum during half this time interval. After the discontinuity, the dichroism and birefringence both take on larger values and show different trends with the dichroism decreasing and the birefringence increasing. Both achieve stable values toward the end of the experiment. The orientation of the initial helix director ($\theta$) at the air−film interface ($z = 0$) was allowed to take on any value as an additional degree of freedom. These results are shown in Figure 11c, as the orientation of the fast axis $\gamma$, where $\gamma = \theta + 90°$. Interestingly, there is a cusp in the data right at the point of the discontinuity. Before this point, $\gamma$ goes through a minimum and then increases; after this point $\gamma$ goes through a maximum and then decreases.

When the data from the experiment using the RCP pump were fit to the same model, the results of the per-layer dichroism and birefringence (shown in Figure 12a) are quite similar to the case of LCP irradiation. Here the birefringence goes through a similar maximum before the discontinuity. For longer exposures, the dichroism and birefringence also level off, but both with the same trend toward larger values. Figure 12b shows the results of the pitch determination. As anticipated, these results mirror those obtained with the opposite pump handedness: now the pitch starts negative and, following a transition at around 80 min of exposure, ends up positive. After the transition, the pitch is seen to decrease from $P = \infty$ before leveling off. This behavior is not observed on the $P < 0$ side of the transition, where the pitch actually increases approaching the discontinuity. Figure 12c shows the values of the initial optical axis orientation at the input face of the helix obtained by the fitting. Here there is also a split between values of $\gamma_{\text{initial}}$ about 80 min exposure.

## 6. Discussion

After examining all of the results obtained from both experiments and both models, some insight into the photoin-

duced chirality in this material may be obtained. The apparent helix reversal during exposure with a fixed handedness of the pump laser will be discussed first, followed by a consideration of the handedness of the structures. The mechanism of the chiral inscription is then discussed and, finally, some further details which may be significant for this material are considered.

**6.1. Helix Reversal.** The most striking feature of the results of fitting the data from the stepwise irradiation experiment to both the uniaxial and helical models is the apparent helix reversal that occurs with a single handedness of the pump laser. In the case of the uniaxial model, this appeared as a change in sign of the parameters $\Delta\alpha_{cir}$ and $\Delta n_{cir}$; with the helix model the reversal was characterized by a change in sign of the pitch. When the pump is LCP, the uniaxial model describes a transition from $\Delta\alpha_{cir}$ and $\Delta n_{cir} < 0$ at short exposures to $\Delta\alpha_{cir}$ and $\Delta n_{cir} > 0$ for longer exposures. Using the helix model, this appears as a transition from $P > 0$ to $P < 0$. Likewise, for irradiation with an RCP pump the trend is reversed: the uniaxial model suggests $\Delta\alpha_{cir}$ and $\Delta n_{cir} > 0$ in the beginning and $\Delta\alpha_{cir}$ and $\Delta n_{cir} < 0$ at saturation; the helix model describes a transition from $P < 0$ to $P > 0$. In the uniaxial model, $\Delta\alpha_{cir}$ and $\Delta n_{cir}$ have approximately the same magnitude before and after the sign change occurs. The helix model provides more insight here: although the total "twisting power" is roughly the same. Before the sign change the pitch is long (around 5000−9000 nm) and the linear anisotropy per layer is larger ($\Delta n_{lin} \approx \pm 0.25$). After the sign change, the helix appears more tightly wound with $P \approx \pm 1500$ nm and the linear anisotropy per layer is smaller ($\Delta n_{lin} \approx \pm 0.15$).

In the mechanism proposed by Nikolova et al.[33,35] the twisting occurs as a result of the change in azimuth of the pump beam as it passes through uniaxially arranged molecules. That is, the linear dichroism and birefringence of the liquid-crystalline sample change the polarization of the pump laser and the azo chromophores respond accordingly, aligning themselves perpendicular to the long axis of the polarization ellipse at each "slice" of the sample thickness. Although the azimuth of the polarization ellipse after passing through the first "layer" is determined by the orientation of the optical axis at the input face of the helix, the sense in which the rotation continues is determined entirely by the handedness of the $Ar^+$ laser. Figure 13 depicts the change in ellipticity of a left-circularly polarized pump beam as it traverses a 3500-$\mu$m sample whose uniaxial anisotropy increases with time/exposure. For small exposures (a), the order parameter within each layer of the sample has just begun to develop and it is seen that by the time the blue light reaches the back of the film, its ellipticity has been significantly reduced from 1.0 to about 0.4. If the exposure continues, the order parameter within the layers increases (b) and so the ellipticity of the pump is affected to a greater extent. Just after it passes through 3 $\mu$m of polymer, it is now linearly polarized ($\tan\omega = 0$), and past this point, for the remaining 500 nm of sample thickness, it travels as a right-circularly polarized ellipse. In this region near the film−glass interface, twisting of the chromophores begins to occur in the opposite sense. When first examining the results of the stepwise irradiation experiment with the uniaxial model, it was thought that the decrease in $\Delta\alpha_{cir}$ and $\Delta n_{cir}$ after the initial maxima was due to homeotropic alignment of the mesogens. Now a second possibility is realized: $\Delta\alpha_{cir}$ and $\Delta n_{cir}$ begin to decrease as an increasing fraction of the helices are wound in the opposite sense. As this trend continues, a point such as (c) may be reached where the pump beam is left- and right-circularly polarized over equal thicknesses in the film. Naturally the resulting circular

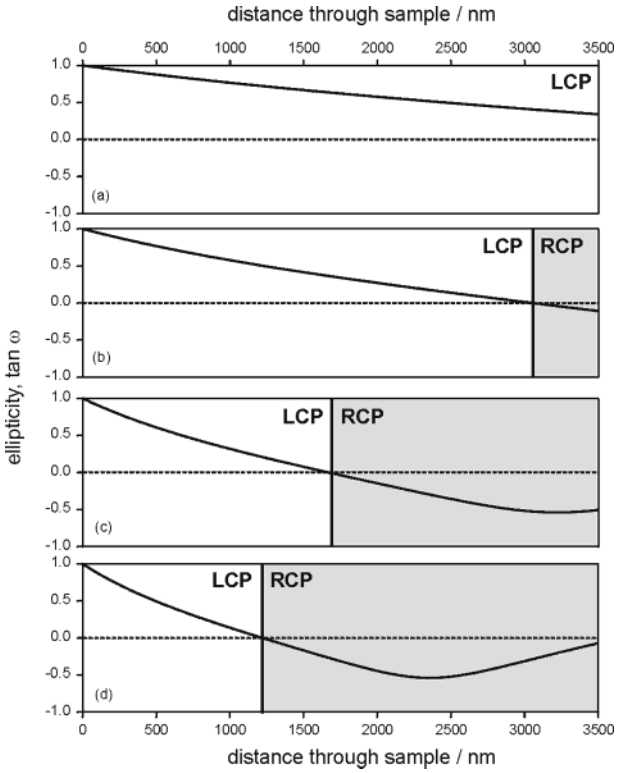


**Figure 13.** As an LCP pump beam traverses a thick uniaxial film, its ellipticity changes as a result of the linear anisotropy. With increasing exposure, the order parameter per layer increases and so the ellipticity is affected to a greater extent. (a) A time early in the exposure with $\Delta\alpha_{lin} = 0.034\ \mu m^{-1}$ and $\Delta n_{lin} = 0.02$. Here the pump beam enters the film as left-circularly polarized and its ellipticity decreases, though all the while remaining left-handed. (b) A bit later in the exposure with $\Delta\alpha_{lin} = 0.067\ \mu m^{-1}$ and $\Delta n_{lin} = 0.04$. Now the pump beam is right-handed for the last small distance through the sample. (c) When $\Delta\alpha_{lin} = 0.13\ \mu m^{-1}$ and $\Delta n_{lin} = 0.75$ the pump changes handedness halfway through the film. (d) If $\Delta\alpha_{lin} = 0.17\ \mu m^{-1}$ and $\Delta n_{lin} = 0.1$ the pump spends most of its time inside the film as a right-handed ellipse.

anisotropy at this point would be zero. Finally, with an even larger amount of linear anisotropy within each layer of the film, the pump, initially LCP upon entering, may travel through more of the sample as RCP than LCP.

There are two interesting cases to consider here which may explain why such a result has not been reported already. The first is that of a thinner sample. Consider the results of Figure 13 again, but this time clipped at the 500 nm mark. As the irradiation progresses and the order parameter evolves from situation (a) through (d), the ellipticity of the pump beam is affected to a greater extent but it remains with its initial handedness. There has not been enough dephasing to switch the sign of the ellipticity. The second case is that of a thick sample which is not as fluid as pMAB6 in its nematic phase, say a smectic LC polymer or an amorphous material that has been prealigned with linearly polarized light. In this case, the linear anisotropy within each layer cannot develop to a large enough extent so, despite the sufficient thickness, the total dephasing of linear components of the polarization is still too small to change the handedness of the pump.

The modeling of the pump ellipticity shown in Figure 13 has not taken into account the response of the mesogens as they reorient toward a direction perpendicular to the long axis of the polarization ellipse. It is difficult to model this process realistically for several reasons. First, the order parameter within a layer is critically affected by the ellipticity of the pump at that point. A much higher order parameter is achieved with

ellipticities closer to zero than with those closer to unity. This resulting order parameter in turn determines the extent to which the azimuth rotates to the next layer. Although these considerations may be approximated relatively simply with a numerical model, the complicating factor in determining the order parameter within the layer is the initial orientation of the director. In cases where movement toward the direction perpendicular to the ellipse long axis requires a small angular change, the final order parameter may be high. On the other hand, if this requires a large change of the existing director, a much smaller degree of ordering might be realized.

**6.2. Handedness of the Helix.** Having addressed the issue of the helix reversal, the attention is now turned toward the question of the overall handedness of the chiral structures. The data from the switching experiment, fitted to the phenomenological model, does not provide any clues on this point since the results merely indicate the sign of the circular dichroism and birefringence for a given handedness of the pump; this is not enough information to determine the absolute configuration of the structure.

The most convincing results come from fitting the stepwise irradiation data with the helix model. Here the polarization data from each time interval could be fit with only one sign for the pitch, either positive or negative. According to the sign conventions used here, a negative value of $P$ is indicative of a right-handed helix; a positive $P$ describes a left-handed helix. This follows the same convention as used to describe the handedness of circularly or elliptically polarized light and is illustrated for the case of a right-handed helix in Figure 3c and d. For irradiation with LCP light, the pitch starts positive and is then negative after the discontinuity. This indicates that, as far as the mechanism is concerned, LCP light results in left-handed winding. The right-handed winding that dominates at long exposures is then attributed to the predominance of right-handed polarization states within the film, as described in the previous section. For irradiation with RCP light, exactly the opposite is observed with a right-handed helix observed first, followed by a left-handed structure at long exposures.

Now consider the results of fitting this same data set to the phenomenological model. Here, just as in the switching experiment, one cannot determine the absolute configuration of the structure from the sign of $\Delta\alpha_{cir}$ or $\Delta n_{cir}$ at a single wavelength. However, examining the orientation of the "average" fast axis $\gamma$ during the irradiation shown for LCP in Figure 9c and for RCP in Figure 10c, a trend may be observed. In both cases, there is an initial plateau region where there is not as great a change in the axis orientation. Afterward, in the case of LCP irradiation, there is a rapid clockwise progression of $\gamma$. This corresponds to a right-handed helix and supports the conclusion based on the pitch determination at long exposures. In the case of RCP exposure, when the axis first begins to change considerably, it is in a counterclockwise sense, supporting the idea that a left-handed structure is being inscribed. Here, however, this trend in $\gamma$ begins shortly before the sign reversal in the pitch, and at long exposures this axis begins to twist in a clockwise manner again.

In the early experimental results from Nikolova's group on photoinduced chirality, it was reported that irradiation with LCP light results in $\Delta\alpha_{cir}$ and/or $\Delta n_{cir} > 0$.[26,28] The authors then made the ad hoc statement that since the handedness of the rotation followed that of the polarized light, the sense of the induced helix should be opposite to that of the pump handedness.[28,33] However, the later quantitative model they developed for the process, which relates the pitch of the structure to the ellipticity of the pump beam, reaches the opposite conclusion.[33,35] In their model, LCP light creates a left-handed helix while RCP light creates a right-handed helix. There are other experiments described in the literature that reach the same conclusions. Kim et al.[36] report that irradiation with left elliptically polarized light rotated the azimuth of the pump in a counterclockwise manner, leading them to suggest that left-handed light produces a left-handed helix. The authors must be careful, however, since it is dangerous to speculate on the structural arrangement of the helix based on the sign of $\Delta n_{cir}$ at a single wavelength. In the study by Iftime et al.[29] $\Delta n_{cir} > 0$ at 632.8 nm, as in the present results, and an assignment of multiple bands in the CD spectrum and subsequent comparison to the spectral results for helical polyisocyanates has resulted in the conclusion that the LCP light used in the study resulted in a left-handed helix.

**6.3. Mechanism of Helix Formation.** The primary feature of Nikolova's proposed mechanism is that the ellipticity of the pump beam is unchanged upon traversing the sample.[33,35] Azzam and Bashara's analysis[34] show that for any given helix with $P > \lambda$ this can only occur for two possible eigenpolarizations with ellipticities governed by the pitch and optical constants of the helix. Nikolova et al. experimentally demonstrate that the transmitted ellipticity is unchanged for a wide range of incident pump ellipticities, and they account for this in their model by showing that the ellipticity of the pump in fact becomes one of the eigenpolarizations of the resulting helix.[33] In the mechanism proposed by Iftime et al., both the azimuth and ellipticity of the pump beam change upon interaction with subsequent smectic layers through the film thickness.[29] Although the evidence presented by Nikolova et al. is compelling, it is difficult to account for the action of a circularly polarized pump beam (tan $\omega = \pm 1$) without relying on a significant change in ellipticity.

At the outset of this study, one of the questions that we had hoped to answer was: what happens during the exposure as the circular anisotropy is seen to increase? There are two possibilities: (1) the helix is becoming more tightly wound with increasing exposure, accounting for the increased $\Delta\alpha_{cir}$ and $\Delta n_{cir}$, and (2) the pitch is somehow fixed at the onset of the exposure and only the order parameter within each layer of the helix increases. That is, the increasing resolution of the helical structure is responsible for the increased circular dichroism and birefringence. Looking at the results of these experiments, there is evidence of both processes occurring simultaneously. There are regions where the phenomenological model shows $\Delta\alpha_{cir}$ and $\Delta n_{cir}$ increasing and the helical model shows the linear order parameters, $\Delta\alpha_{lin}$ and $\Delta n_{lin}$ within the layers, increasing while the pitch at the same time decreases. On the other hand, the results at times show tradeoffs between layer ordering and pitch which result in the same twisting power. Still, it is quite astonishing that the pitch does not vary more than what is actually determined here. The values of pitch that fit the data at the very beginning of the exposure are essentially constant (at least within the same order of magnitude) until the switch-over point. At this stage, it is difficult to say whether this is a shortcoming of the model or a realistic picture of the structures inscribed in the film.

**6.4 Other Considerations.** In previous studies with liquid crystalline materials, Nikolova et al. have already mentioned that the presence of many domains with a large distribution of directors may lead to multiple helices inscribed in the sample.[33] This is a very likely situation here since there is no surface treatment on the glass substrate prior to casting the film and so the sample is textured, or multidomain. The many helices will have their helical axes parallel to each other and are anticipated

to have very similar pitches, but will differ primarily in the orientation of the optical axes at the input face, $\gamma_{initial}$. There is another type of order parameter, then, which governs the distribution of these different types of helices. Although the directors of each domain in the addressed area before irradiation have a fixed orientation, they will likely change during the inscription process. This is likely the reason there is not a smooth progression of $\gamma_{initial}$ with exposure in Figures 11c and 12c. Of all the order parameters modeled and tracked in these experiments, this one is the most susceptible to there being more than one helix in the irradiated area. Still, the inclusion of this parameter was necessary to better determine $\Delta\alpha_{lin}$, $\Delta n_{lin}$, and the pitch since the angular shift in the Stokes parameter $S_3(\beta)$ was often very far from that of $S_1$ and $S_2$.

Although the circular birefringence and dichroism show the same trend when the stepwise irradiation data was fit with the phenomenological model, in the case of the RCP irradiation the zero crossing occurs at exactly the same moment while for LCP irradiation the dichroism changes sign first, followed by the birefringence almost 1 h later. This LCP−RCP data set was chosen since it is representative of the results obtained for many identical experiments: whenever the experiment was performed, there is typically some amount of angular shift between the positions where $\Delta\alpha_{cir}$ and $\Delta n_{cir}$ cross zero. Such a shift is strange, but provides an explanation for some of the behavior observed in repeated switching experiments. It was occasionally noticed that for long irradiation cycles (ca. 1 h) the values of $\Delta\alpha_{cir}$ and $\Delta n_{cir}$ for a given handedess of the pump had opposite signs. This was puzzling since, whatever the values of $\Delta\alpha_{cir}$ and $\Delta n_{cir}$, it is expected that they necessarily have the same sign for a given structure. Now it seen that when the irradiation happens to fall in the transition region bound by the two dashed lines in Figure 9a, these anisotropic parameters may have opposite signs.

## 7. Conclusions

When polarized light is incident on helical structures, the transmission shows evidence of linear and circular anisotropy. When the liquid-crystalline polymer pMAB6 was irradiated with circularly polarized light, the appearance of circular anisotropy whose sign depended on the handedness of the pump suggested that a chiral configuration of chromophores was induced. Two models have been described. In the first model, the linear anisotropy is treated as being uniaxial and circular anisotropy is included at the phenomenological level. In the second model, a helix is built from a twisted-stack of linear absorbers/retarders. Switching of the circular anisotropy was demonstrated by changing the polarization of the pump in LCP−RCP cycles and fitting the resulting transmission polarization data to the uniaxial model. Then the handedness of the pump was fixed and the film was irradiated in 5-min intervals so that the evolution of the ordered structures could be monitored. These data were fit to both the uniaxial and helix models. Assignment of the configuration of the resulting structures which likely resemble disordered helices cannot be made based on the sign of the circular dichroism or optical rotation at a single wavelength (and this task is still tricky with data over multiple wavelengths), but the results obtained here provide some unambiguous support for the conclusion that left-circularly polarized light induces left-handed helical segments, and right-circularly polarized-light inscribes right-handed segments.

With both models, there appears to be a rather sharp discontinuity during the exposure where the sign of the circular anisotropy or the pitch of the helix changes. Since (1) the films used in this study have appreciable thickness and (2) a high local order parameter may be achieved due to a nematic phase, a large phase shift between linear components of the (initially) circularly polarized pump occurs. It is proposed that while travelling inside the film, the handedness of the pump may change as a result of this dephasing, and a segment of the helix is created with the opposite handedness than that of the initial inscription.

**Acknowledgment.** The polymer pMAB6 was prepared by Dr. Yiliang Wu, a postdoctoral fellow in our lab, currently at the Xerox Research Centre of Canada. We thank the Natural Science and Engineering Research Council of Canada, and the Department of National Defence (Canada) for funding this work. D.H. thanks the Government of Ontario for an Ontario Graduate Scholarship.

## References and Notes

(1) Delaire, J. A.; Nakatani, K. *Chem. Rev.* **2000**, *100*, 1817.
(2) Kumar, G. S.; Neckers, D. C. *Chem. Rev.* **1989**, *89*, 1915.
(3) Todorov, T.; Nikolova, L.; Tomova, N. *Appl. Opt.* **1984**, *23*, 4309.
(4) Ho, M.-S.; Natansohn, A.; Rochon, P. *Macromolecules* **1995**, *28*, 6124.
(5) Natansohn, A.; Rochon, P.; Ho, M.-S.; Barrett, C. *Macromolecules* **1995**, *28*, 4179.
(6) Ikeda, T.; Tsutsumi, O. *Science* **1995** *268*, 1873.
(7) Ikeda, T.; Tsutsumi, O.; Wu, Y. *Mol. Cryst. Liq. Cryst.* **2000**, *347*, 1.
(8) Shishido, A.; Tsutsumi, O.; Ikeda, T. *Mater. Res. Soc. Symp. Proc.* **1996**, *425*, 213.
(9) Shishido, A.; Kanazawa, A.; Shiono, T.; Kanazawa, A.; Ikeda, T.; Tamai, N. *J. Mater. Chem.* **1999**, *9*, 2211.
(10) Dalton, L. R.; Steier W. H.; Robinson, B. H.; Zhang, C.; Ren, A.; Garner, S.; Chen, A.; Londergan, T.; Irwin, L.; Carlson, B.; Fifield, L.; Phelan, G.; Kincaird, C.; Amend, J.; Jen, A. *J. Mater. Chem.* **1999**, *9*, 1905.
(11) Denning, R. G. *J. Mater. Chem.* **2001**, *11*, 19.
(12) Natansohn, A.; Rochon, P. *Can. Chem. News* **2000**, June, 18.
(13) Sabi, Y.; Yamamoto, M.; Watanabe, H.; Bieringer, T.; Haarer, D.; Hagen, R.; Kostromine, G. G.; Berneth, H. *Jpn. J. Appl. Phys.* **2001**, *40*, 1613.
(14) Reringa, B. L.; van Delden, R. A.; Koumura, N.; Geertsema, E. M. *Chem. Rev.* **2000**, *100*, 1789.
(15) de Vries, H. *Acta Crystallogr.* **1951**, *4*, 219.
(16) Mayer, S.; Zentel, R. *Macromol. Rapid Commun.* **2000**, *21*, 927.
(17) Mayer, S.; Maxein, G.; Zentel, R. *Macromolecules* **1998**, *31*, 8522.
(18) Mayer, S.; Zentel, R. *Macromol. Chem. Phys.* **1998**, *199*, 1675.
(19) Mruk, R.; Zentel, R. *Macromolecules* **2002**, *35*, 185.
(20) Bobrovsky, A. Y.; Boiko, N. I.; Shibaev, V. P. *Chem. Mater.* **2001**, *13*, 1998.
(21) Bobrovsky, A. Y.; Boiko, N. I.; Shibaev, V. P.; Prudnikova, E.; Torgova, S. I. *Liq. Cryst.* **2000**, *27*, 1381.
(22) Ruslim, C.; Ichimura, K. *Adv. Mater.* **2001**, *13*, 37.
(23) Ruslim, C.; Ichimura, K. *J. Phys. Chem. B* **2000**, *104*, 6529.
(24) Kurihara, S.; Nomiyama, S.; Nonoka, T. *Chem. Mater.* **2001**, *13*, 1992.
(25) Kurihara, S.; Nomiyama, S.; Nonaka, T. *Chem. Mater.* **2000**, *12*, 9.
(26) Nikolova, L.; Todorov, T.; Ivanov, M.; Andruzzi, F.; Hvilsted, S.; Ramanujam, P. S. *Opt. Mater.* **1997**, *8*, 255.
(27) Nikolova, L.; Todorov, T.; Ivanov, M.; Andruzzi, F.; Hvilsted, S.; Ramanujam, P. S. *Appl. Opt.* **1996**, *35*, 3835.
(28) Naydenova, I.; Nikolova, L.; Ramanujam, P. S.; Hvilsted, S. *J. Opt. A: Pure Appl. Opt.* **1962**, *1*, 438.
(29) Iftime, G.; Lagugné Labarthet, F.; Natansohn, A.; Rochon, P. *J. Am. Chem. Soc.* **2000**, *122*, 12646.
(30) Angiolini, L.; Caretti, D.; Giorgini, L.; Salatelli, E. *Macromol. Chem. Phys.* **2000**, *201*, 533.
(31) Berova, N., Kananishi, K., Woody, R. W., Eds. *Circular Dichroism: Principles and Applications*; Wiley-VCH: New York, 2000.
(32) Ivanov, M.; Naydenova, I., Todorov, T.; Nikolova, L.; Petrova, T.; Tomova, N.; Dragostinova, V. *J. Mod. Opt.* **2000**, *47*, 861.
(33) Nikolova, L.; Nedelchev, L.; Todorov, T.; Petrova, T.; Tomova, N.; Dragostinova, V.; Ramanujam, P. S.; Hvilsted, S. *Appl. Phys. Lett.* **2000**, *77*, 657.
(34) Azzam, R. M. A.; Bashara, N. M. *Ellipsometery and Polarized Light*; North-Holland Publishing Company: New York, 1977.

(35) Nedelchev, L.; Nikolova, L.; Todorov, T.; Petrova, T.; Tomova, N.; Dragostinova, V.; Ramanujam, P. S.; Hvilsted, S. *J. Opt. A: Pure Appl. Opt.* **2001**, *3*, 304.
(36) Kim, M.-J.; Chin, B.-G.; Kim, J.-J.; Kim, D.-Y. *J. Am. Chem. Soc.* **2002**, *124*, 3504.
(37) Kasha, M.; Rawls, H. R.; El-Bayoumi, M. A. *Pure Appl. Chem.* **1965**, *11*, 371.
(38) Birabassov, R.; Galstian, T. *J. Opt. Soc. Am. B* **2001**, *18*, 1469.
(39) Ichimura, K.; Ham, M. *Chem. Lett.* **2000**, 286.
(40) Angeloni, A. S.; Caretti, D.; Carlini, C.; Chiellini, E.; Galli, G.; Altomare, A.; Solaro, R. *Liq. Cryst.* **1989**, *4*, 513.
(41) Hatada, K.; Kitayama, T.; Nishiura, T.; Tawada, M.; Harazono, T.; Sugaya, T. *J. Macromol. Sci.* **1997**, *A34*, 1183.
(42) Hore, D.; Natansohn, A.; Rochon, P. *J. Phys. Chem. B*, submitted.
(43) Hore, D.; Natansohn, A.; Rochon, P. *J. Phys. Chem. B* **2002**, *106*, 9004.
(44) Jones, R. C. *J. Opt. Soc. Am.* **1948**, *38*, 671.
(45) Kriezis, E. E.; Elston, S. J. *Liq. Cryst.* **1999**, *26*, 1663.
(46) Yu, F. H.; Kwok, H. S. *J. Opt. Soc. Am. A* **1999**, *16*, 2772.
(47) Marathay, A. S. *J. Opt. Soc. Am.* **1971**, *61*, 1363.
(48) Berreman, D. W. *J. Opt. Soc. Am.* **1972**, *62*, 502.
(49) Stallinga, S. *J. Appl. Phys.* **1999**, *85*, 3023.
(50) Merrill, B. E.; Azzam, R. M. A.; Bashara, N. M. *J. Opt. Soc. Am.* **1974**, *64*, 731.
(51) Azzam, R. M. A.; Merrill, B. E.; Bashara, N. M. *Appl. Opt.* **1973**, *12*, 764.
(52) Azzam, R. M. A.; Bashara, N. M. *J. Opt. Soc. Am.* **1972**, *62*, 1252.
(53) Berreman, D. W.; Scheffer, T. J. *Mol. Cryst. Liq. Cryst.* **1970**, *11*, 395.
(54) Oseen, C. W. *Trans. Faraday Soc.* **1933**, *29*, 883.
(55) Ichimura, K.; Han, M.; Morino, S. *Chem. Lett.* **1999**, 85.
(56) Han, M.; Morino, S.; Ichimura, K. *J. Photopolym. Sci. Technol.* **1999**, *12*, 289.
(57) Han, M.; Ichimura, K. *Macromolecules* **2001**, *34*, 82.
(58) Wu, Y.; Ikeda, T.; Zhang, Q. *Adv. Mater.* **1999**, *11*, 300.